nature climate change

LETTERS

https://doi.org/10.1038/s41558-019-0507-8

Cloud microphysics and circulation anomalies control differences in future Greenland melt

Stefan Hofer[1,2*], Andrew J. Tedstone[1], Xavier Fettweis[2] and Jonathan L. Bamber[1]

Recently, the Greenland Ice Sheet (GrIS) has become the main source of barystatic sea-level rise[1,2]. The increase in the GrIS melt is linked to anticyclonic circulation anomalies, a reduction in cloud cover and enhanced warm-air advection[3–7]. The Climate Model Intercomparison Project fifth phase (CMIP5) General Circulation Models (GCMs) do not capture recent circulation dynamics; therefore, regional climate models (RCMs) driven by GCMs still show significant uncertainties in future GrIS sea-level contribution, even within one emission scenario[5,8–10]. Here, we use the RCM Modèle Atmosphèrique Règional to show that the modelled cloud water phase is the main source of disagreement among future GrIS melt projections. We show that, in the current climate, anticyclonic circulation results in more melting than under a neutral-circulation regime. However, we find that the GrIS longwave cloud radiative effect is extremely sensitive to the modelled cloud liquid-water path, which explains melt anomalies of +378 Gt yr^{-1} (+1.04 mm yr^{-1} global sea level equivalent) in a +2 °C-warmer climate with a neutral-circulation regime (equivalent to 21% more melt than under anticyclonic circulation). The discrepancies between modelled cloud properties within a high-emission scenario introduce larger uncertainties in projected melt volumes than the difference in melt between low- and high-emission scenarios[11].

Clouds are of first-order importance for the GrIS surface energy budget (SEB; Supplementary equation (1))[12,13]. For shortwave (SW) fluxes, clouds (1) block incoming solar radiation and (2) change the albedo of the surface[12,13]. The amount of solar radiation reaching the surface for vertically homogeneous liquid clouds depends on the cloud optical depth (COD, $\tau = (3\mathrm{LWP})/(2\rho_w r_e)$), which is a function of the liquid-water path (LWP), the effective particle radius (r_e) and the density of water (ρ_w). The variability in the LWP controls the variability in the COD. Clouds interact with the surface by filtering parts of the near-infrared spectrum where the ice albedo is low, thereby increasing the broadband surface albedo[13].

For longwave (LW) fluxes, clouds contribute to the SEB by trapping heat, depending on the cloud phase[14]. Although clouds tend to warm the high albedo interior of the GrIS[15], the secular trend in enhanced melt over the darker ablation zone is partly controlled by a decrease in summer cloud cover and increased SW downward (SWD) radiation and net shortwave radiation (SWnet)[4]. These complex interactions show that an appropriate representation of cloud microphysics is critical for reducing uncertainties in the projected GrIS sea-level contribution[2,4,12,14,16–18].

To analyse the differences between the RCP8.5 GrIS melt projections, we forced the RCM Modèle Atmosphèrique Règional (MAR)[6] with three different projections from the CMIP5 model suite[6,19,20]. We chose these GCMs because they most closely match the 700 hPa temperature and mid-tropospheric circulation over Greenland from 1980 to 1999 when compared with the European Centre for Medium-Range Weather Forecasting (ECMWF) reanalysis (ERA) product ERA-Interim[19]. However, because the CMIP5 models do not predict the recent anticyclonic circulation regime over Greenland[4,5,10,19], these results are only valid for a neutral-circulation state.

There is a marked difference in the total melt amount between the simulations (Fig. 1). From 2017 to 2100 (projected), the MAR forced by the second generation Canadian Earth System Model (CanESM2) simulates 86,000 Gt of melt anomalies (23.7 cm sea-level equivalent (SLE)[21]) during summer (June, July, August; JJA), almost twice as much as the MAR forced by the Norwegian Earth System Model (NorESM1) (46,400 Gt, 12.8 cm SLE) and the Model for Interdisciplinary Research on Climate Version Five (MIROC5) (54,100 Gt 14.9 cm SLE). There is a factor of 1.85 between the smallest and largest melt projections; this factor is larger than 1.75, which is the difference between the projected GrIS contributions to barystatic global sea-level rise by the end of the twenty-first century under RCP 2.6 and RCP 8.5 (ref. [11]).

The most notable energy flux contribution comes from the JJA longwave downward (LWD) radiation anomalies, equating to 79,400 Gt melt potential between 2017 and 2100 in the CanESM2. Again, the NorESM1 and the MIROC5 show notably lower LWD anomalies, with 59,300 Gt and 58,300 Gt, respectively. The significant positive correlation between melt and LWD anomalies explains between 86% and 95% of melt anomalies (Supplementary Fig. 1). Conversely, SWD anomalies are negative across all simulations. These correlations suggest that the SW transmissivity of the atmosphere will decrease in a warming climate with a neutral circulation over the GrIS[22]. This combined change in LWD and SWD anomalies points towards a contribution from cloud microphysical properties.

Despite a decrease in SWD, SWnet anomalies are positive in all simulations because of the melt-albedo feedback[3,23]. The CanESM2 also estimates the largest increase in SWnet at 36,200 Gt, versus 19,300 Gt (NorESM1) and 26,900 Gt (MIROC5). We find that SWD and SWnet anomalies are of second-order importance in future GrIS surface mass balance (SMB) projections compared to differences in LWD (on average, SWnet is 2.4 and SWD 2.1 times lower)[22]. Although the albedo scheme of the MAR has been verified against in-situ observations and remote sensing data, the quantification of the SWnet anomalies remains subject to uncertainties because the MAR lacks important albedo feedbacks[23–26].

There are two mechanisms that physically explain the differences in LW fluxes: differences in (1) the emissivity of the atmosphere (equation (1)) and (2) air temperature. Because infrared cloud emissivity (ϵ) is linked to cloud microphysics and the COD (τ) via

$$\epsilon = 1 - \exp(-\beta\tau) \quad (1)$$

[1]School of Geographical Sciences, University of Bristol, Bristol, UK. [2]Laboratory of Climatology, Department of Geography, University of Liège, Liège, Belgium. *e-mail: s.hofer@bristol.ac.uk

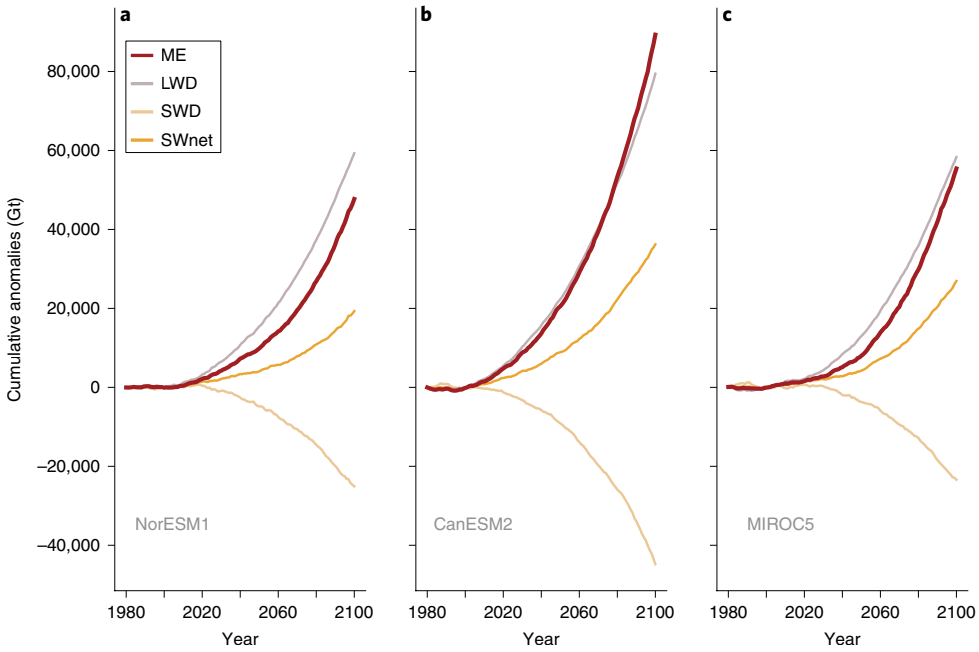

Fig. 1 | Cumulative summer melt and radiation anomalies expressed as melt potential. a–c, Cumulative anomalies based on the 1980–1999 mean state of the model expressed as melt anomalies (Gt) and radiation anomalies as melt potential (Gt), with MAR forced by NorESM1 (**a**), with CanESM2 input (**b**) and with MIROC5 input (**c**). ME represents the cumulative melt anomaly, SWD and LWD the shortwave downward and longwave downward anomalies and SWnet the anomaly in the net shortwave radiation.

where β is a diffusivity factor[27], any increase in the COD may also enhance the general LWD fluxes from the atmosphere by increasing the emissivity.

Figure 2 (first row) shows that the CanESM2, which produces the highest projected melt and LWD anomalies, also shows the largest increase in COD: 2.18 times greater than that of the NorESM1 and 2.06 times greater than that of the MIROC5 (1980–2100). The increase in all three simulations correlates most closely with a quadratic increase of the COD over time.

The MAR CanESM2 also predicts the largest increase in LWD anomalies, reaching 1,165 Gt (NorESM1), 1,622 Gt (CanESM2) and 1,122 Gt (MIROC5; Fig. 2, second row).

All three simulations show a statistically significant positive correlation between the COD and LWD ($R^2 = 0.98$, 0.99 and 0.99; Fig. 2, last row). However, the increase in the COD is defined by a second order polynomial, whereas the anomalies in the LWD show a more linear response, indicating a saturation effect. Using the equation of the saturation curve (Fig. 2, last row), we find that the impact of the COD on LWD anomalies would cease when the COD equals 1.46 (CanESM2), 0.61 (NorESM1) and 0.57 (MIROC5). At these points, the cloud emissivity reaches unity in a neutral future GrIS circulation state. Figure 2 (last row) also indicates a transient response of the LW cloud radiative effect, with a decreasing sensitivity with increasing COD. However, in our simulations cloud cover does not change during the twenty-first century and, therefore, increasing COD is the only mode of variability. Normally, the atmospheric emissivity only reaches unity when the cloud cover approaches 100%. Conversely, an increase in COD beyond the saturation values for LWD would still reduce SWD anomalies because this effect saturates more slowly[14]. These results also suggest that the LW cloud radiative effect is currently highly sensitive to changes in cloud properties (that is, there is a steep slope at the current COD).

The representation of atmospheric water content is very important in determining the SEB because the LW emissivity of clouds (equation (1)) is dominated by variability in the LWP. Figure 3a–c shows only small differences in the total ice-water path (IWP), with averages of 62, 67 and 60 g m^{-2}. However, there are notable differences in the LWP, with the MAR CanESM2 estimating a 2.7 times greater LWP. The optically thicker clouds in the highest melt simulation are therefore due to a markedly larger amount of liquid water, rather than a homogeneous increase in both IWP and LWP. This marked difference in cloud liquid water path also highlights how COD and higher melt are connected: the MAR CanESM2 produces clouds that bear more liquid water, which leads to optically thicker clouds via $\tau = (3\mathrm{LWP})/(2\rho_w r_e)$, which in turn makes the atmosphere more efficient at emitting LWD (compare with equation (1)). The source of higher LWP and melt in the CanESM2-forced run may be associated with higher humidity as CanESM2 predicts an earlier ice-free Arctic Ocean than other CMIP5 models[28]. The GCMs in the Arctic region are also highly sensitive to tropical teleconnections and differences in ocean forcing such as the Atlantic Multidecadal Oscillation[29,30].

We are confident that the LW emissivity is not influenced by changes in the overall JJA cloud cover. Although the cloud cover shows marked decadal variability, there is no clear secular trend (Supplementary Fig. 2a), probably because the GCMs do not simulate future circulation changes[10,19].

Temperature only accounts for small proportions of LW and melt anomalies. At the start, the MAR CanESM2 (the model with 1.85 times more melt) ranks in second place for melt season temperature (2 m above ground), whereas MIROC5 is the warmest (Supplementary Table 1 and Supplementary Fig. 2b,c). The MAR CanESM2 also has the coldest annual temperature at the start. However, the MAR CanESM2 becomes slightly warmer towards the end of the twenty-first century when its JJA temperature is elevated by 0.9 °C and 1.8 °C compared to the MIROC5 and NorESM1 simulations, respectively. These differences in the JJA temperatures are probably a consequence of and not a precursor for differences in modelled cloud microphysics. When the atmosphere is approximated as a black body (Supplementary equation (2)) (from 2080 to 2100), these temperature anomalies only explain 2.7% of the differences in LWD.

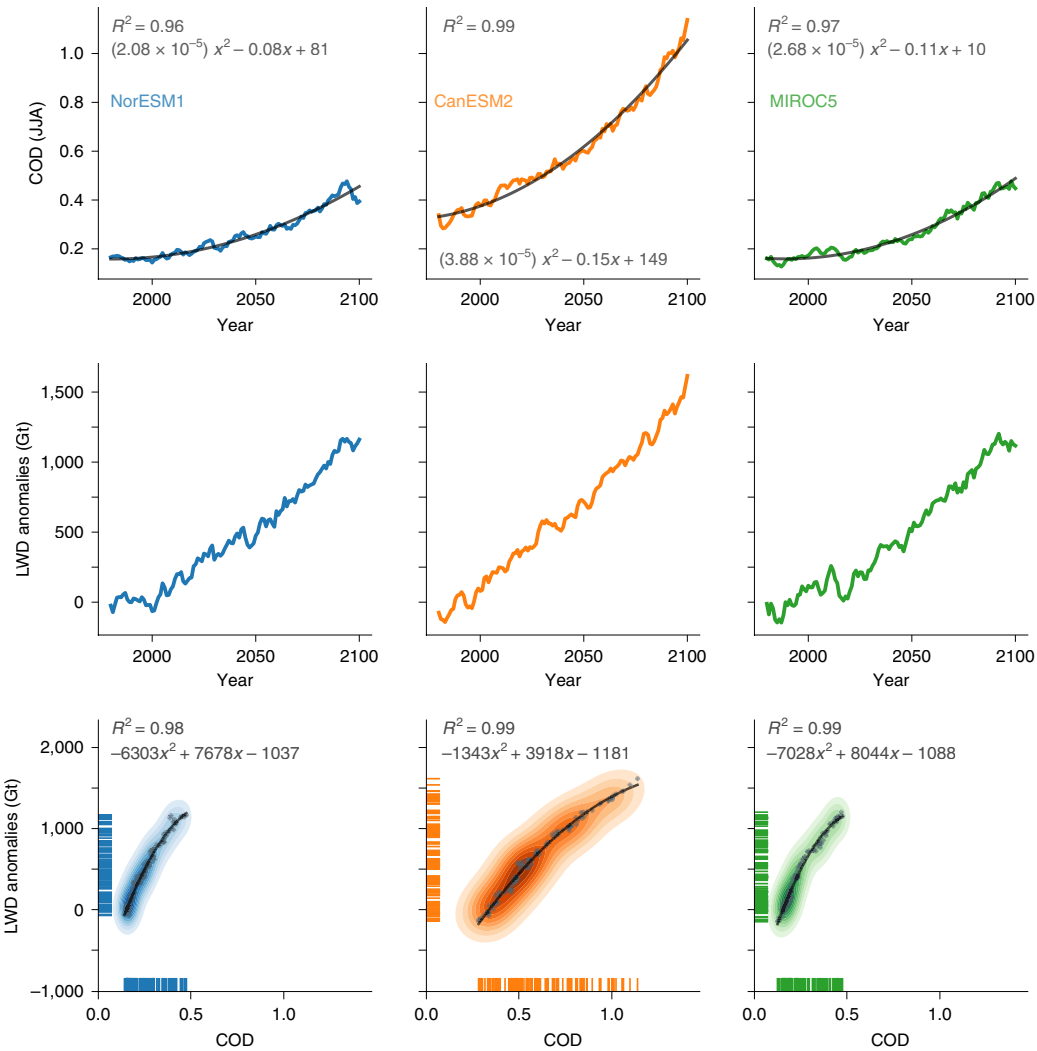

Fig. 2 | Cloud optical depth, LWD and their connection. The first row shows the five-year running mean of COD during JJA over the GrIS from the three different GCM inputs: NorESM1, CanESM2 and MIROC5 from left to right (blue, orange and green, respectively). The black line is a second-order polynomial fit, with corresponding second order polynomial equations and R^2 values as plot labels ($P \ll 0.01$). The second row shows the five-year running mean of GrIS JJA LWD anomalies based on the 1980–1999 mean state of the model, expressed as melt potential (Gt). The last row shows the correlation between JJA COD and LWD anomalies with a second-order polynomial fit to the data and corresponding fit parameters and R^2 values ($P \ll 0.01$).

The MAR is able to reproduce the JJA cloud-cover trends when compared to satellite data with increases in the north and decreases in the south of Greenland[4]. We also checked the MAR's ability to reproduce observed cloud LWP and atmospheric water-vapour content when forced with the ERA-Interim[31–33]. Although the MAR slightly underestimates the LWP between autumn and spring when compared to observations from Summit, Greenland[31,32], it accurately captures the LWP evolution during the melt season. The MAR also accurately models the precipitable water-vapour distribution over Summit (Fig. 3e).The MAR therefore captures the influence of cloud water-phase distribution on the SEB and future GrIS melt.

In addition to cloud microphysics, missing circulation anomalies in the GCMs are a second major source of uncertainties[5,10]. The recent melt increase over the GrIS is largely attributed to a switch of the North Atlantic Oscillation to an anticyclonic state[4,5,7,10,34,35]. These circulation anomalies have led to a decrease in cloud cover and to an increase in warm-air advection mainly over southwestern Greenland, increasing both LW and SW fluxes[3–5]. However, the latest studies show that all the CMIP5 models used for future projections do not simulate these circulation anomalies[7,10]. Delhasse et al.[5] have shown that future melt could double if anticyclonic circulation were to persist during the twenty-first century.

To compare uncertainties resulting from potentially missing anticyclonic circulation anomalies with uncertainties due to cloud microphysics, we forced the MAR with artificially warmed reanalysis data, which capture the recent anticyclonic circulation anomalies because they are observationally constrained[6,19,35]. We examined the effect of anticyclonic circulation anomalies on the GrIS melt and the SEB anomalies at different warming levels (+0 °C, +1 °C, +1.5 °C, +2 °C between 1980 and 1999) and compared them to differences due to modelled cloud microphysics in a neutral future Greenland circulation (Fig. 4). We compared the results from two periods—1980 to 1999 and 2000 to 2016—when circulation anomalies were observed at four warming levels (see Methods). We note that the period from 2000 to 2016 is 0.7 °C warmer than the reference period due to an inseparable combination of (1) circulation changes causing warm-air advection and (2) global warming.

Furthermore, we compare one RCP 8.5 simulation that produces the most twenty-first century melt (CanESM2) to the mean of the other two projections at the same warming levels to assess differences resulting from diverging cloud LWP (see Methods).

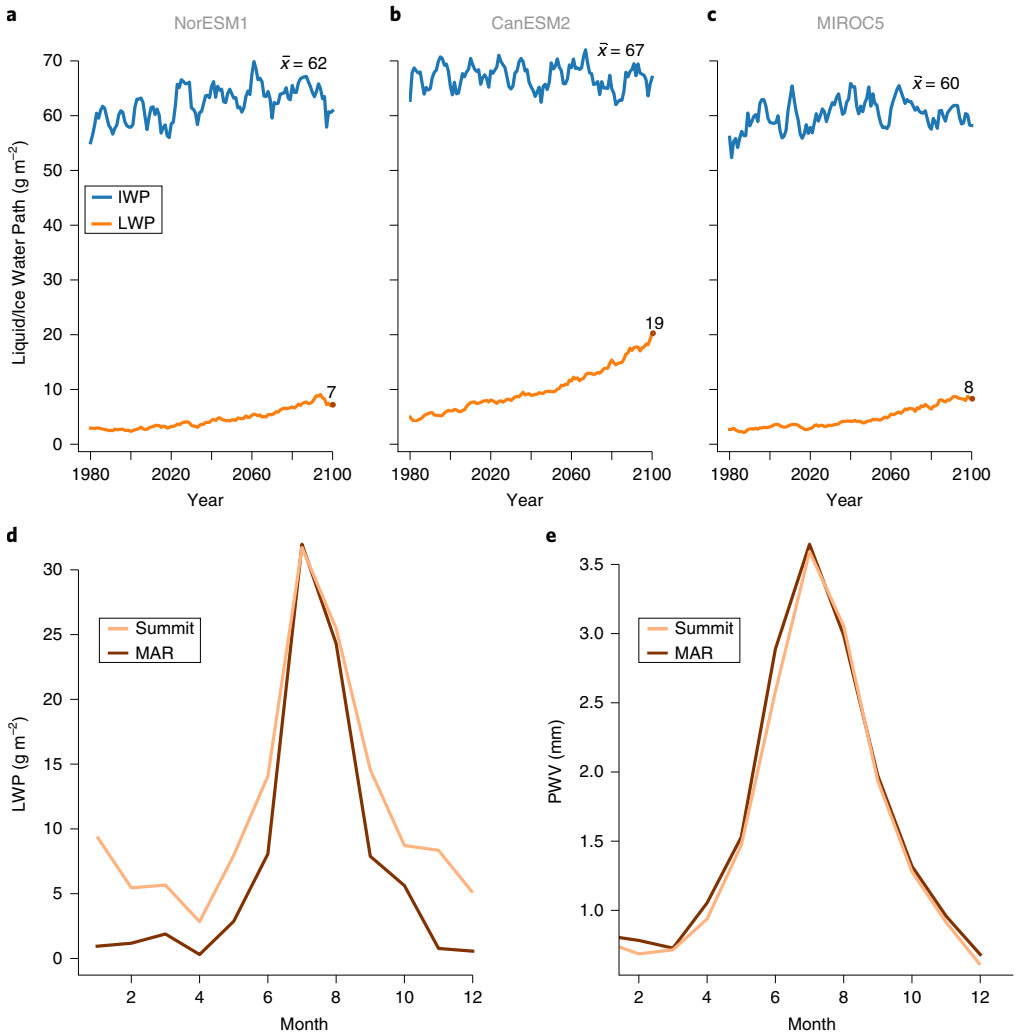

Fig. 3 | Evolution of LWP and IWP and comparison to in-situ and satellite observations. a–c, The five-year rolling mean of the JJA LWP and IWP over Greenland between 1980 and 2100. $\bar{x}$ indicates the average of the IWP over the entire time series (1980–2100). **d**, A comparison of the annual LWP (g m^{-2}) cycle for Summit, Greenland. We compare the monthly mean annual cycle MAR LWP over Summit (72°35′46.4″ N 38°25′19.1″ W) to in-situ observations from Summit between January 2011 and June 2014 when in-situ data are available[31,32]. **e**, The monthly mean annual precipitable water vapour (PWV) cycle from the MAR over Summit and in-situ observations from Summit.

Our results therefore show the melt signal resulting from cloud microphysics on top of the additional melt due to tropospheric warming.

At the present-day climate of +0 °C, anticyclonic circulation anomalies are 4.7 times more efficient at enhancing melt than cloud LWP anomalies at +218 Gt yr^{-1} compared to +38 Gt yr^{-1} (Fig. 4a). The higher melt sensitivity to anticyclonic circulation anomalies is principally because anticyclonic circulation may enhance both LWD fluxes (warm-air/humidity advection) and SWD fluxes (cloud dissipation)[4,5]. Conversely, positive LWP anomalies can only enhance the LWD, whereas the SWD is being reduced due to cloud optical thickness (Fig. 4b,c).

The extra melt due to uncertainties in modelled cloud microphysics is more sensitive to increasing temperatures than melt due to anticyclonic circulation anomalies. At +2 °C, the cloud liquid-water response yields an increase in melt of +378 Gt yr^{-1} (+1.04 mm yr^{-1} SLE[21]), a tenfold increase from the +38 Gt yr^{-1} at +0 °C. Melt due to anticyclonic circulation anomalies only increases by a factor of 1.4 compared to +0 °C, resulting in +311 Gt yr^{-1} (+0.86 mm yr^{-1}). Although a LW-dominated SEB could potentially lead to more melt over the bright accumulation zone and less melt over the darker ablation zone, we do not find any strong evidence for this: at +2 °C in the anticyclonic case, 83% of total melt occurs in the ablation zone, compared to 82% in the neutral CanESM2 simulation. The main reason for the higher sensitivity of the neutral-circulation case is an increase in the LWD by a factor of 1.6 and an increase in the SWnet (Fig. 4d) from −121 Gt yr^{-1} to +39 Gt yr^{-1} due to the melt-albedo feedback, despite negative SWD anomalies (Fig. 4b). However, the SWD anomalies decrease more slowly than the rate of LWD increase, implying a different sensitivity of the LW and SW downwelling fluxes to cloud microphysics in a warming climate.

Partitioning the SEB and comparing two distinctly different GrIS circulation scenarios enables us to show that major uncertainties in future GrIS sea-level contribution arise from two different pathways. First, anticyclonic circulation anomalies may add an additional +311 Gt yr^{-1} (+0.86 mm yr^{-1} SLE) in a +2 °C warmer climate (in addition to the increase in melt by increased temperature alone) by increasing both SW fluxes (via reduced clouds in the south) and LW fluxes (via enhanced temperature/humidity advection and more clouds in the north). However, it is unclear whether recent anticyclonic circulation anomalies will persist during the twenty-first century. Second, in a more neutral Greenland

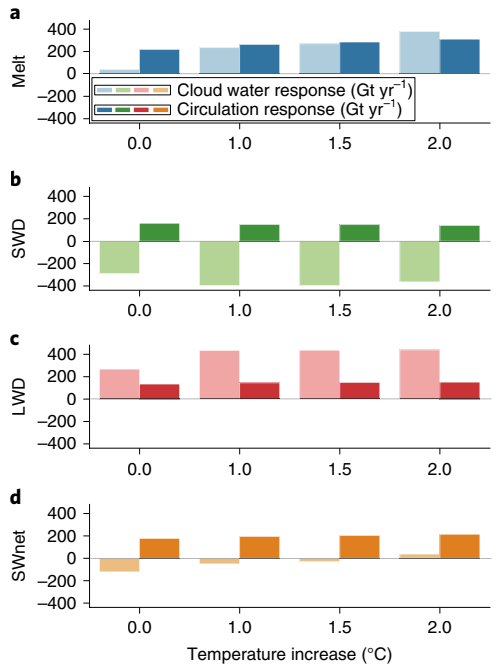

Fig. 4 | Impact of anticyclonic circulation anomalies and cloud liquid-water fraction anomalies on melt and the SEB. a, Impact of circulation anomalies (dark blue) and LWP anomalies (pale blue) on JJA melt and surface-energy flux anomalies (Gt yr^{-1}) at different temperatures compared to 1980 to 1999 (+0 °C, +1 °C, +1.5 °C and +2 °C). Anomalies due to circulation changes are based on comparing the 1980 to 1999 mean of MAR forced by ERA-Interim with the 2000 to 2016 period where circulation anomalies have been observed. The cloud liquid-water response is calculated on the basis of comparing the mean of two MAR projections forced with GCMs without markedly enhanced cloud liquid-water fraction (MIROC5 and NorESM1) with MAR CanESM2, which shows notably enhanced cloud LWP. **b**–**d**, Impact of circulation and cloud liquid-water fraction anomalies on SWD flux anomalies (**b**), LWD anomalies (**c**) and absorbed SWnet fluxes (**d**) expressed as melt potential (Gt yr^{-1}).

circulation state, notable uncertainties arise from differences in modelled cloud microphysics and downwelling LW fluxes; the potential exists to contribute +378 Gt yr^{-1} (+1.04 mm yr^{-1} SLE) at +2 °C in addition to the melt increase due to tropospheric warming. These melt anomalies are closely linked to the LW cloud radiative effect, which is currently highly sensitive to an increase in the COD. Our results indicate that uncertainties due to cloud processes depend on the specific circulation pathway and that the cloud radiative effect shows a transient response in a warming climate (Supplementary discussion). In conclusion, our study highlights two key areas that should be addressed to greatly reduce GrIS melt uncertainties: (1) improvement of cloud microphysics and radiative schemes in climate models based on higher density of in-situ observations of clouds' water phase, and (2) understanding the drivers of current GrIS circulation anomalies to assess the likelihood of their persistence in the future.

Online content

Any methods, additional references, Nature Research reporting summaries, source data, statements of code and data availability and associated accession codes are available at https://doi.org/10.1038/s41558-019-0507-8.

Received: 4 September 2018; Accepted: 14 May 2019;
Published online: 24 June 2019

References

1. Van Den Broeke, M. R. et al. On the recent contribution of the Greenland ice sheet to sea level change. *Cryosphere* **10**, 1933–1946 (2016).
2. van den Broeke, M. et al. Greenland ice sheet surface mass loss: recent developments in observation and modeling. *Curr. Clim. Change Rep.* **3**, 345–356 (2017).
3. Box, J. E. et al. Greenland ice sheet albedo feedback: thermodynamics and atmospheric drivers. *Cryosphere* **6**, 821–839 (2012).
4. Hofer, S., Tedstone, A. J., Fettweis, X. & Bamber, J. L. Decreasing cloud cover drives the recent mass loss on the Greenland Ice Sheet. *Sci. Adv.* **3**, e1700584 (2017).
5. Delhasse, A., Fettweis, X., Kittel, C., Amory, C. & Agosta, C. Brief communication: impact of the recent atmospheric circulation change in summer on the future surface mass balance of the Greenland Ice Sheet. *Cryosphere* **12**, 3409–3418 (2018).
6. Fettweis, X. et al. Reconstructions of the 1900–2015 Greenland ice sheet surface mass balance using the regional climate MAR model. *Cryosphere* **11**, 1015–1033 (2017).
7. Hanna, E., Cropper, T. E., Hall, J. & Cappelen, J. Greenland blocking index 1851–2015: a regional climate change signal. *Int. J. Climatol.* **4861**, 4847–4861 (2016).
8. Taylor, K. E., Stouffer, R. J. & Meehl, G. A. An Overview of CMIP5 and the experiment design. *B. Am. Meteorol. Soc.* **93**, 485–498 (2012).
9. Knutti, R. & Sedláček, J. Robustness and uncertainties in the new CMIP5 climate model projections. *Nat. Clim. Change* **3**, 369–373 (2013).
10. Hanna, E., Fettweis, X. & Hall, R. J. Brief communication: recent changes in summer Greenland blocking captured by none of the CMIP5 models. *Cryosphere* **12**, 3287–3292 (2018).
11. Church, J. et al. in *Climate Change 2013: The Physical Science Basis* (eds Stocker, T. F. et al.) 1137–1216 (IPCC, Cambridge Univ. Press, 2013).
12. Bintanja, R. & Van Den Broeke, M. R. The influence of clouds on the radiation budget of ice and snow surfaces in Antarctica and Greenland in summer. *Int. J. Climatol.* **16**, 1281–1296 (1996).
13. Warren, S. G. Optical properties of snow. *Rev. Geophys.* **20**, 67 (1982).
14. Shupe, M. D. & Intrieri, J. M. Cloud radiative forcing of the Arctic surface: the influence of cloud properties, surface albedo, and solar zenith angle. *J. Climate* **17**, 616–628 (2004).
15. Van Tricht, K. et al. Clouds enhance Greenland ice sheet meltwater runoff. *Nat. Commun.* **7**, 10266 (2016).
16. Bennartz, R. et al. July 2012 Greenland melt extent enhanced by low-level liquid clouds. *Nature* **496**, 83–86 (2013).
17. Bony, S. et al. CFMIP: Towards a better evaluation and understanding of clouds and cloud feedbacks in CMIP5 models. *Clivar Exch.* **56**, 20–22 (2011).
18. Tsay, S. et al. Radiative energy budget in the cloudy and hazy Arctic. *J. Atmos. Sci.* **46**, 1002–1018 (1989).
19. Fettweis, X. et al. Estimating the Greenland ice sheet surface mass balance contribution to future sea level rise using the regional atmospheric climate model MAR. *Cryosphere* **7**, 469–489 (2013).
20. Fettweis, X., Tedesco, M., Van Den Broeke, M. & Ettema, J. Melting trends over the Greenland ice sheet (1958–2009) from spaceborne microwave data and regional climate models. *Cryosphere* **5**, 359–375 (2011).
21. IPCC *Climate Change 2013: The Physical Science Basis* (eds. Stocker, T. F. et al.) Annex iii: Glossary (Cambridge Univ. Press, 2013).
22. Franco, B., Fettweis, X. & Erpicum, M. Future projections of the Greenland ice sheet energy balance driving the surface melt. *Cryosphere* **7**, 1–18 (2013).
23. Tedesco, M. et al. The darkening of the Greenland ice sheet: trends, drivers, and projections (1981–2100). *Cryosphere* **10**, 477–496 (2016).
24. Tedstone, A. J. et al. Dark ice dynamics of the south-west Greenland Ice Sheet. *Cryosphere* **11**, 2491–2506 (2017).
25. Alexander, P. M. et al. Assessing spatio-temporal variability and trends in modelled and measured Greenland Ice Sheet albedo (2000–2013). *Cryosphere* **8**, 2293–2312 (2014).
26. Cook, J. M. et al. Quantifying bioalbedo: a new physically based model and discussions of empirical methods for characterising biological influence on ice and snow albedo. *Cryosphere* **11**, 2611–2632 (2017).
27. Curry, J. A. & Ebert, E. E. Annual cycle of radiation fluxes over the Arctic Ocean: sensitivity to cloud optical properties. *J. Climate* **5**, 1267–1280 (1992).
28. Stroeve, J. C. et al. Trends in Arctic sea ice extent from CMIP5, CMIP3 and observations. *Geophys. Res. Lett.* **39**, L16502 (2012).
29. Trenberth, K. E., Fasullo, J. T., Branstator, G. & Phillips, A. S. Seasonal aspects of the recent pause in surface warming. *Nat. Clim. Change* **4**, 911–916 (2014).
30. Ding, Q. et al. Tropical forcing of the recent rapid Arctic warming in northeastern Canada and Greenland. *Nature* **509**, 209–12 (2014).
31. Miller, N. B. et al. Cloud radiative forcing at Summit Greenland. *J. Clim.* **28**, 6267–6280 (2015).
32. Miller, N. B. et al. Surface energy budget responses to radiative forcing at Summit, Greenland. *Cryosphere* **11**, 497–516 (2017).

33. Dee, D. P. et al. The ERA-Interim reanalysis: configuration and performance of the data assimilation system. *Q. J. Roy. Meteor. Soc.* **137**, 553–597 (2011).
34. Hanna, E. et al. Atmospheric and oceanic climate forcing of the exceptional Greenland ice sheet surface melt in summer 2012. *Int. J. Climatol.* **34**, 1022–1037 (2014).
35. Fettweis, X. et al. Brief communication: important role of the mid-tropospheric atmospheric circulation in the recent surface melt increase over the Greenland ice sheet. *Cryosphere* **7**, 241–248 (2013).

Acknowledgements

This work was supported by the National Environment Research Council (grant no. ME/M021025/1) and received funding from the European Research Council under the European Union's Horizon 2020 research and innovation programme under grant agreement no. 694188. This work was also supported by the Fonds de la Recherche Scientifique (FNRS) and the Fonds Wetenschappelijk Onderzoek-Vlaanderen (FWO) under the EOS Project n° O0100718F. For the MAR simulations, computational resources were provided by the Consortium des Equipements de Calcul Intensif, funded by the Fonds de la Recherche Scientifique de Belgique (F.R.S.-FNRS) under grant no. 2.5020.11, and the Tier-1 supercomputer (Zenobel) of the Fèdèration Wallonie-Buxelles, and infrastructure was funded by the Walloon Region under grant agreement no. 1117545. X.F. is a research associate of the F.R.S.-FNRS. S.H. would like to thank M. McCrystall for valuable discussions on the topic.

Author contributions

S.H. analysed the data and wrote the manuscript. S.H., J.B. and A.T. designed the study and methods. J.B. and A.T. supervised the project. X.F. developed and provided the daily climate model outputs as well as additional analyses. All authors discussed the results and commented on the manuscript.

Competing interests

The authors declare no competing interests.

Additional information

Supplementary information is available for this paper at https://doi.org/10.1038/s41558-019-0507-8.

Reprints and permissions information is available at www.nature.com/reprints.

Correspondence and requests for materials should be addressed to S.H.

Peer review information: *Nature Climate Change* thanks Ruth Mottram, Matthew Shupe and the other, anonymous, reviewer(s) for their contribution to the peer review of this work.

Publisher's note: Springer Nature remains neutral with regard to jurisdictional claims in published maps and institutional affiliations.

Methods

Supplementary discussion. The analysis presented here has potential consequences on the degree to which clouds influence current and future melt[4,15,36] and specifically on how we discuss the GrIS cloud radiative effect.

First, in a neutral-circulation state and corresponding climate, the changes and uncertainties in the SEB are mostly due to a 'pure' cloud effect, with competing downwelling fluxes in the SW and LW part of the spectrum. Here, 'pure' means that the response in the SEB is controlled by changes only in cloud cover or microphysics. 'Pure' cloud effects can only ever enhance one of the two fluxes whereas the other part is reduced; therefore, the exact value of the cloud radiative effect is important. However, our analysis and the previous results (Fig. 2, bottom and ref. [14]) show that the impact of clouds on the SEB is far from constant over time in a changing climate. In the LW part, the GrIS is currently extremely sensitive to any increase in the COD; however, the response flattens as the cloud LW emissivity (ϵ) reaches unity. Conversely, the reductions in the SW part are less sensitive to an increase in the COD, leading to a transient cloud radiative effect that is being dominated by downwelling LW fluxes. However, in a warming climate the SW impact does not saturate as quickly as in the LW; therefore, with further warming the CRE influence could become SW-dominated (again). It is therefore essential to consider, especially with rising temperature levels due to greenhouse gas emissions, that the GrIS CRE is not constant over time and is also showing a transient response. Any value attributed to it is only valid for the specific time period considered and not as a general constant.

Second, anticyclonic circulation anomalies over Greenland during the past 20 years have increased both SW and LW fluxes, with SW fluxes being the dominant contribution over this period[4]. However, there are two potential mechanisms that could have led to this signal that need further investigation. First, increases in LW and SW fluxes over the same geographical areas could be due to a 'mixed' response from decreases in cloud cover (more SW) and a higher frequency of warm-air and moisture advection (more LW). In this case, the exact quantification of the cloud radiative effect might be of lower importance because it is theoretically possible to have positive SW and LW anomalies under cloud cover reductions in areas where clouds would usually warm the surface. Second, the positive SW and LW flux anomalies may be explained by recent studies[4] that have focused on a GrIS-wide aggregation of anomalies. GrIS-wide aggregation of radiation anomalies could mask the importance of the observed differences in cloud cover trends over geographically and climatologically separate areas of the GrIS, with increases in clouds over the cold and dry north and decreases in cloud cover over the south, where clouds over the ablation zone have been found to cool the surface in summer[36,37]. Therefore, we think that additional studies on the effect of clouds on the Greenland SEB and SMB (in hindcast simulations) should take a basin-scale approach when discussing recent trends in cloud characteristics.

Modèle Atmosphèrique Règional. The RCM used in this study, the MAR, is a non-hydrostatic atmospheric model that solves the primitive equation set. A detailed description of the model setup, physics and performance in regional climate simulations is given in refs. [6,38,39]. In this study, we used the MAR v3.9.0 . The forcing fields from the CMIP5 model data[8] are prescribed at the model boundaries at a 6-h timestep for (1) the period 1976 to 2100 for the MIROC5 and NorESM1 forcing fields and (2) the period 1971 to 2100 for the CanESM2 forcing fields. These fields include information about temperature, wind, humidity and pressure at the surface. Within the model, the one-dimensional energy-balance-based snow model, Soil Ice Snow Vegetation Atmosphere Transfer (SISVAT), creates links between the atmosphere, snowpack, permanent ice (on glaciers and the ice sheet) and the tundra surrounding the GrIS[40]. The physical properties of snow and ice in SISVAT are directly based on the snow model CROCUS[40,41]. The model was run on an equal-area grid with a 25 km resolution when forced by GCMs (future projections) and with a 15 km resolution when forced by reanalysis data. Over the GrIS, the MAR has been extensively tested and its physics have been finely tuned to match in-situ and remote sensing data. Furthermore, the MAR was also tested against other polar RCMs[6,20,38]. It has been especially tuned to match the surface mass balance and melt extent on the GrIS[20,38]. The cloud scheme of the MAR was first developed based on ref. [42], with marked improvements being implemented on the basis of work performed during the Mixed-Phase Arctic Cloud Experiment[43].

Sensitivity to anticyclonic circulation anomalies and cloud microphysics. *ERA-Interim sensitivity experiments.* To assess the impact of anticylonic circulation anomalies over Greenland as observed during the past two decades, we split the ERA-Interim reanalysis product[33] into two parts following Delhasse et al.[5]. First, the JJA 1980 to 1999 period served as the reference period in which no circulation anomalies were observed and the GrIS was in equilibrium[1,44]. Second, we used the JJA 2000 to 2016 period, when anticyclonic circulation anomalies were observed, to examine the impact of anticylonic conditions on melt and radiative fluxes relative to the neutral-circulation reference period. We note that the period from 2000 to 2016 was 0.7 °C warmer than the reference period due to an inseparable combination of (1) circulation changes causing warm-air advection and (2) global warming. In the next step, we artificially increased the ERA-Interim temperature at all of the 24 vertical sigma levels of the MAR by +1 °C, +1.5 °C and +2 °C. We preserved the relative humidity at the lateral boundaries by increasing the specific humidity. Sea surface conditions remained unchanged in the warmed ERA-Interim input fields. In Fig. 4 all the comparisons labelled 'Circulation response' are differences between the 1980 to 1999 period (neutral circulation) and the 2000 to 2016 period where anticylonic circulation anomalies were observed. Positive values correspond to higher melt or radiative fluxes during the anticyclonic period from 2000 to 2016.

GCM sensitivity tests. We compared the response of GrIS radiation fluxes and melting caused by anticyclonic circulation anomalies (see ERA-Interim sensitivity experiments) to the response caused by diverging modelled cloud water phase in the GCM-forced MAR simulations at different warming levels. First, for each of the MIROC5- and NorESM1-forced MAR simulations, we identified each 20-year period where the mean JJA temperature (at 850, 700, 600 and 500 hPa) over the whole integration domain reached +1 °C, +1.5 °C and +2 °C compared to the 1980–1999 reference period. Next, we calculated the mean 20-year period of the two simulations for each warming level. We used these mean 20-year periods to compute the mean of the radiative fluxes and melt at +0 °C (1980–1999), +1 °C, +1.5 °C and +2 °C for each of the three GCM-forced simulations.

To identify the radiation and melt anomalies associated with cloud microphysics alone (that is, without associated tropospheric warming), we compared the mean radiative and melt fluxes of the MIROC5- and NorESM1-forced simulations (low LWP enhancement, Fig. 3a,c) with the CanESM2-forced simulation (~3 × LWP enhancement compared to the other simulations, Fig. 3b) at each warming level and period identified. We note that the CanESM2 exhibited slightly more JJA warming at each period or warming level than the other two simulations (Supplementary Tables 1 and 2). During the whole period of study, the CanESM2 projects approximately 1 °C more warming over Greenland (Supplementary Table 1, ΔT). However, the CanESM2-forced JJA temperatures are in agreement with the other simulations during the 1980 to 1999 reference period; we therefore conclude that the higher rate of warming through the CanESM2-forced simulation is due to a positive feedback with the higher amount of liquid-water content and greater downwelling LW radiation, rather than a warm-bias inherent to the CanESM2 simulation.

Computation of anomalies. Anomalies presented in this paper are calculated based on the 1980 to 1999 average of the model outputs (melt, SMB, cloud properties, radiative properties and so on). Whenever radiation anomalies and non-radiative SEB components are not shown using their SI unit (joule), they have been converted to a mass anomaly ('melt potential')[4]. For this purpose, we use the heat of fusion that is needed to melt 1 kg of ice, $H_f = 333.55\,\mathrm{kJ\,kg^{-1}}$, where positive values correspond to an above-average downward flux of energy or heat. A positive anomaly therefore means that more energy has been received at the surface of the GrIS than in the reference climate period. The radiative scheme in the MAR is the same that used in the ERA-40 reanalysis product[45]. Radiative fluxes in the SW and LW are broadband values integrated over the whole range of the corresponding spectrum.

The three steps from the model output on the $25 \times 25\,\mathrm{km^2}$ grid to the anomalies are as follows:

- Computing the monthly arithmetic mean of a given parameter from daily model outputs
- Computing the climatological mean state of every pixel for every month from 1980 to 1999
- Summing up the anomalies from the climatological mean and converting to melt potential (if applicable)

The following equation was used to compute the anomalies for every pixel and month:

$$a_{i,j,\mathrm{month}} = x_{i,j,\mathrm{month}} - \overline{x_{i,j,m}} \quad (2)$$

where $a_{i,j,\mathrm{month}}$ refers to the anomaly of a model pixel value ($x_{i,j,\mathrm{month}}$) in the ith rows and jth column of the grid, from the corresponding monthly grid-cell climatology. Subscript m refers to the month for which the equation was evaluated, and subscript i and j refer to the specific position on the model grid. We began with the radiative anomalies at each pixel in $\mathrm{W\,m^{-2}}$. Because of the grid-cell extent of $25 \times 25\,\mathrm{km^2}$, we then multiplied the radiative anomalies by the area of the pixel to arrive at the total anomaly in watts (joules per second) of one singular grid cell. We then summed up all the values spatially over the entire GrIS (see equation (3)) and multiplied the spatially aggregated radiation anomalies (joules per second) by the duration of the month (in seconds). This took us from joules per second to the total anomalies in joules, which we then converted to melt anomalies in gigatons:

$$\Delta a_{\mathrm{total}} = \sum_i \sum_j a_{i,j,\mathrm{month}} \quad (3)$$

CMIP5 and RCPs. The CMIP5 is the most recently completed GCM intercomparison project[8]. Overall, more than 20 climate modelling groups contributed, using more than 50 different models[8]. To produce a higher resolution

RCM output, the Coordinated Regional Downscaling Experiment (CORDEX) was built around the CMIP5 GCM model output[8], with the MAR model outputs used in the CORDEX downscaling experiment being compliant with the CORDEX framework[6]. For the CMIP5 models, there are four formulated RCPs, but only two of them are part of the 'core' experiments in the CMIP5 project[8]. The RCP values (for example, in RCP 8.5) refer to the approximate forcing due to atmospheric greenhouse gases in $W\,m^{-2}$ at the surface of the Earth compared to pre-industrial levels[8]. The RCP 8.5 pathway used in this study is a high-emission scenario ('business as usual'), with the radiative forcing increasing throughout the twenty-first century[8]. Various other intercomparison projects have been built around the CMIP5, with one specifically looking at feedbacks from clouds in the GCMs (Cloud Feedback Model Intercomparison Project; see ref. [17]). However, despite a notable increase in resolution (and therefore more computational power being used by these models) and more physical processes being captured by the CMIP5 model block compared to previous CMIP models, the overall spatial and temporal patterns of main climate variables such as temperature and precipitation have not changed markedly[9]. The CMIP5 models have incorporated more physical processes than any other CMIP project before, making it the best representation of climate change modelling based on physical characteristics to date[8,9].

Data availability

The monthly means from 1980 to 2100 of all three MAR RCP 8.5 simulations used in this study are available via ftp://ftp.climato.be/fettweis/MARv3.9/Greenland/. If daily outputs are required, they can be requested from X.F. (xavier.fettweis@uliege.be) and S.H.

Code availability

All the code used for the analysis in this study is available upon request from the corresponding author.

References

36. Wang, W., Zender, C. S. & van As, D. Temporal characteristics of cloud radiative effects on the Greenland ice sheet: discoveries from multiyear automatic weather station measurements. *J. Geophys. Res.-Atmos.* **123**, 11,348–11,361 (2018).
37. Wang, W., Zender, C. S., van As, D. & Miller, N. B. Spatial distribution of melt-season cloud radiative effects over Greenland: evaluating satellite observations, reanalyses, and model simulations against in-situ measurements. *J. Geophys. Res.-Atmos.* **124**, 57–71 (2018).
38. Fettweis, X. Reconstruction of the 1979–2006 Greenland ice sheet surface mass balance using the regional climate model MAR. *Cryosphere* **1**, 21–40 (2007).
39. Gallee, H. & Schayes, G. Development of a three-dimensional meso-γ primitive equation model: katabatic winds simulation in the area of Terra Nova Bay, Antarctica. *Mon. Weather Rev.* **122**, 671–685 (1994).
40. De Ridder, K. & Gallée, H. Land surface–induced regional climate change in Southern Israel. *J. Appl. Meteorol.* **37**, 1470–1485 (1998).
41. Gallée, H., Guyomarc'h, G. & Brun, E. Impact of snow drift on the Antarctic ice sheet surface mass balance: possible sensitivity to snow-surface properties. *Bound.-Lay. Meteorol.* **99**, 1–19 (2001).
42. Meyers, M. P., DeMott, P. J. & Cotton, W. R. New primary ice-nucleation parameterizations in an explicit cloud model. *J. Appl. Meteorol.* **31**, 708–721 (1992).
43. Fridlind, A. M. et al. Ice properties of single-layer stratocumulus during the mixed-phase Arctic cloud experiment: 2. model results. *J. Geophys. Res.* **112**, D24201 (2007).
44. van den Broeke, M. et al. Partitioning recent Greenland mass loss. *Science* **326**, 984–986 (2009).
45. Uppala, S. M. et al. The ERA-40 re-analysis. *Quart. J. R. Meteorolog. Soc.* **131**, 2961–3012 (2005).